Neurology, Psychiatry and Brain Research 31 (2019) 1–8

Contents lists available at ScienceDirect

Neurology, Psychiatry and Brain Research

journal homepage: www.elsevier.com/locate/npbr

Transit phases of β-amyloid and tau proteins formation and re-solubilisation in AD rat hippocampus tissue as probed by ATR-IR spectroscopy

Maha Jameal Balgoon[a], Gehan A.-R. Ahmed[a,b,*], Safaa Y. Qusti[b], Soad Shaker[c]

[a] Biochemistry Department, Faculty of Science, King Abdulaziz University, Jeddah, Saudi Arabia
[b] Spectroscopy Department, Physics Division, National Research Centre, Dokki, Giza, Egypt
[c] Faculty of medicine, King Abdulaziz University, Jeddah, Saudi Arabia

ARTICLE INFO

Keywords:
Attenuated total reflection-infrared spectroscopy (ATR-IR)
Alzheimer's disease (AD)
Rat hippocampus
β-Amyloid (Aβ)
Hierarchical cluster analysis (HCA)
Congo red stain

ABSTRACT

Objectives: Alzheimer's disease (AD) was believed to be mainly due to the accumulation of free radicals that trigger the membrane peroxidation and protein oxidation in brain tissue. The mechanism of β-amyloid (Aβ) formation, aggregation in $AlCl_3$ induced AD in hippocampus rat brain tissue, the curative and the protective effects of *Lepedium sativum* (LS) water extract as a natural anti-inflammatory, antioxidant and as acetylcholinesterase inhibitor were explored.

Materials and methods: Adult Albino male Wistar rats rat divided into; control, AD, curative, protective, and LS groups (n = 20). Hippocampus tissue were studied histologically and spectroscopically by ATR-IR.

Results: Many significant changes in band position, area and half band width of the resultant decomposed bands between AD and the other tested groups. The α-helix band in the raw spectra was resolved into two distinct sub-bands around 1651 and 1659 cm^{-1} with different percentage areas in all tested groups and in the random coil sub-band as well. A hypothesis on how Aβ is formed and re-solubilized through transit α-helix and random coil formation was postulated in response to LS treatment. In AD rat hippocampus tissue, a significant marked degenerative change was observed in the hippocampal neurons. Most cells appeared smaller, shrunk, deformed and pyknotic nuclei that stained deeply by Congo red. In curative group, the amount of degenerated cells markedly decrease compared to AD group. The intensity of Congo red stained cells was decreased.

Conclusion: This study gave a highlight on the therapeutic effect of LS that can manage Aβ formation and re-solubilisation on AD rat model.

1. Introduction

Increased oxidative stress (OS) is a widely accepted participant in the development and progression of multiple diseases. OS is associated with many conditions such as aging as well as diseases such as Alzheimer's disease (AD) cancer, cardiovascular diseases, diabetes (both type I and type II).

AD is a progressive neurodegenerative disorder, its pathological hallmarks are known to be due to the deposition of extracellular beta-amyloid proteins (Aβ) together with the formation of intracellular neurofibrillary tangles (NFTs) (highly phosphorylated tau proteins) (Korte, Herrmann, Zhang, & Draguhn, 2012). As a result of Aβ neurotoxicity, synaptic loss, dysfunction and neural death happened in the hippocampal and cerebral cortical regions (Haass, Kaether, Thinakaran, & Sisodia, 2012).

The lipid peroxidation and degradation chain reaction proceeds when lipids are attacked by free radicals that lead to broken chemical bonds, cross-linkages, and conformational changes of different biomolecular substances and protein (Cakmak, Zorlu, Severcan, & Severcan, 2011). Aluminum (Al) compound has a great affinity to bio-membrane and has the ability to promote formation and aggregation of insoluble Aβ. For that reason, Al is well-known as a neurotoxin agent (Shati, Elsaid, & Hafez, 2011). Various neurodegenerative diseases such as AD and Parkinsonism disease are strongly linked to Al. Aluminum can bind to different metal binding proteins that influences homeostasis of other metals (Kumar & Gill, 2014). Aluminum may exert its neurotoxicity via free radical production and peroxidation damage to lipids and proteins (Sethi, Jyoti, Singh, Hussain, & Sharma, 2008). Chronic aluminum exposure has the ability to promote formation and aggregation of insoluble Aβ plaques and (NFTs) in Alzheimer brain. Al exposure is

* Corresponding author at: Spectroscopy Department, Physics Division, National Research Centre, 33El Bohouth St. (former El Tahrir St.), Dokki, P.O. 12622, Giza, Egypt.
E-mail address: gehan_raouf@hotmail.com (G.A.-R. Ahmed).

https://doi.org/10.1016/j.npbr.2018.11.001
Received 4 July 2018; Received in revised form 22 October 2018; Accepted 6 November 2018
Available online 15 November 2018
0941-9500/

associated with impairment of mitochondrial functions and antioxidant defense system, *in vivo* and *in vitro* (Kumar, Bal, & Gill, 2008; Kumar, Bal, & Gill, 2009) and a decreases in the antioxidant enzyme status (Esparza et al., 2005).

In our previous study (Balgoon, Raouf, Qusti, & Ali, 2015) we investigated in detail the hippocampus membrane lipid peroxidation and alteration in membrane physical properties mediated by $AlCl_3$ and assessed the therapeutic ability of LS water extract. In this study, the protein oxidation and misfolding, induced by Al treatment in AD rat hippocampus tissues, was extensively studied together with the assessment of the curative and protective effects of LS water extract probed by ATR-IR spectroscopy and histological studies.

2. Materials and methods

The experimental work of the present study was conducted at the King Fahd Medical Research Centre, Medical Biophysics Laboratory-King Abdulaziz University, Jeddah, Saudi Arabia.

2.1. Chemicals

All chemicals, in the present study were in the pure form purchased from SIGMA ALDRICH chemical company, St. Louis, USA supplied. *Lipidium sativum* (LS) seeds obtained from the local herbalist shops in Jeddah.

2.2. Animal and experimental design

One hundred albino male Wistar rats with a body weight ranged between 200–250 g m. were housed in plastic cages in a room with a relative humidity of 70%, temperature of (24 ± }1 °C), and exposed to a light and dark cycle of 12 h duration. The rats were acclimatized for one week before the experiment started. The current study was approved by the Animal House, King Fahd Medical Research Centre, King Abdulaziz University. All applicable international, national and/or institutional guidelines for the care and use of animals were followed. Five groups of rats with a minimum of 20 rats per each were sorted randomly. Control (Cont), AD ($AlCl_3$), curative (Cure), protective (Prot), and positive control (LS). AD was induced to rats by administration of ($AlCl_3$) intraperitoneal (IP) (10 mg/kg of body weight) daily to groups AD, Cure, Prot; Cont and LS groups injected (IP) normal saline instead. Groups Cure, Prot and LS received orally 20 mg/kg of body weight LS water extract while groups Cont and AD were receiving orally normal saline. All rats received standard rat pellet form Grain Silos and Flour Mills Organization, Jeddah, Saudi Arabia and water as beverage. Diet and water were supplied ad-libitum.

2.3. Brain tissue sampling and preparation

Three rats from each group were fasted overnight, rats were euthanized following light ether anaesthesia. The skull was opened carefully and the whole brain of each rat was rapidly removed. The brain was quickly dissected into 2 halves; one was fixed in 10% neutral buffered formalin for further histopathological examination. Hippocampus from the other half was dissected out according to procedure documented by (Drury & Wallington, 1980). The hippocampus tissues washed with saline, immediately immersed in Eppendorf tubes in liquid nitrogen and stored at −80 °C until use. All samples were lyophilized, and gently grounded in agate mortar prior to ATR-IR measurement.

2.4. Attenuated total Reflection-IR

For each sample (ATR-IR) spectrum was recorded in absorbance form using Perkin Elmer Spectrum 100 instrument in the wavenumber range of 4000–400 cm^{-1} with an average of 40 scans and spectral resolution of at 4 cm^{-1}. Background spectra, which were collected under identical conditions, were subtracted from the sample spectra automatically. For each examined sample, the final spectrum was represented by co-added the three spectra as the average of three different measurements. All spectra were baseline corrected and normalized to the entire spectrum by using OMNIC software program. In order to increase the resolution of the overlapping bands a Gaussian decomposition was used to localize the position of the bands in the row spectra by using the same software.

2.5. Histopathological examination

Tissues fixed in neutral buffered formalin (10%) were further processed for cleared in xylene and embedded in paraffin embedding in a hot air oven at 561oC for 24 h. Paraffin bees wax blocks were prepared for sectioning at 4 mm using a microtome. Five-micron sagittal sections of brain tissue were stained with haematoxylin and eosin (H&E) stains for general structure and Congo red for amyloid substance. Histopathological changes were evaluated using a light microscope (Downie, 1990).

2.6. Statistical analysis

The ATR-IR spectral differences among the groups under investigation were determined by using multivariate exploratory techniques. Hierarchical cluster analysis (HCA) was used to compare the spectra of Cont, $AlCl_3$, and all LS treated groups to determine if there were some underlying structural differences (Abeysekara, Damiran, & Yu, 2013). It is the simplest and most rapid procedure of cluster analysis that is used to classify data of ATR-IR. This method depends on the similarity between two objects (Forina, Armanino, & Raggio, 2002). HCA were performed using PAST software. The multivariate classification (data recognition) was performed between the intensities of the collected IR bands. The software used were OMNIC 8.3.103 for the manipulation of IR spectra and used for curve fitting. For the ATR-IR, data were represented as their mean value ± standard error. The differences between Cont, $AlCl_3$, and all LS treated groups were analysed using the *t*-test for independent measurement. A $P < 0.05$ was considered as significant.

3. Results

3.1. ATR-IR measurements

The average absorption infrared spectra from three different rat brains hippocampus were obtained from each group as shown in (Fig. S1). The main spectrum absorption bands belonged mainly to the cellular components of lipids, proteins, carbohydrates and nucleic acids. The absorption band assignments are given in (Table 1) according to the literature (Akkas, Inci, Zorlu, & Severcan, 2007; Kumar & Gill, 2014; Palaniappan & Vijayasundaram, 2009). Particularly, the use of spectroscopic techniques is focused here on the bimolecular changes in protein content and protein secondary structure.

Curve fitting of the average spectrum obtained from each group over 1800–1500 cm^{-1} regions was performed in order to segregate between the overlapped bands as shown in (Fig. 1). The band position, intensity, area and half band width (HBW) of the resultant amide I (1600–1700 cm^{-1}) sub-bands are given in Table S1.

For further investigation of the amide I region near 1652 cm^{-1}, which gives information about the whole protein secondary structure of the cell, the percentage area of the amide I protein sub-bands were calculated in Table 2 with their band assignments. The α-helix band around 1652 cm^{-1} is clearly resolved into two distinct α-helix sub-bands around 1651 and 1659 cm^{-1}. It is obvious from the Table that the β-parallel pleated sheet band around 1688 cm^{-1}, detected in both the control and all LS treated groups, disappeared only in $AlCl_3$ group.

Table 1
Proposed band assignments of the ATR-IR spectra of hippocampus rat brain tissue in the 3030-500 cm^{-1} spectral range.

Wave number(WN) (cm^{-1})	Band assignments
3293.6	Amide A: mainly N−H stretching of proteins
3065	Amide B: N−H stretching of proteins
3013.47	Olefinic HC═CH stretching of alkene: lipids
2956	CH_3 asymmetric stretch: mainly lipids
2923	CH_2 antisymmetric stretch: mainly lipids
2852.38	CH_2 symmetric stretch: mainly lipids
1739.81	Carbonyl C═O stretch: lipids
1651.42	Amide I: C═O stretching of proteins
1545.33	Amide II: N−H bending and C−N stretching of proteins
1466.55	CH_2 bending stretch: mainly lipids
1388	C═O stretch of COO− symmetric stretch: fatty acids and amino acids
1307.36	Amide III,(N-H) bending in plane and C−H stretch
1234.95	PO^{2-} asymmetric stretch: mainly phospholipids
1170.32	Ester CO−O−C asymmetric stretching: phospholipids, triglycerides and cholesterol esters
1066.11	PO^{2-} symmetric stretch: mainly nucleic acids; HO−C−H stretch: carbohydrates : polysaccharides, glycolipids andstretch C−O−P
972.85	Str :C−O; *trans*. RCH═CHR,C−H, bending C—N —C stretch: nucleic acids, ribose-phosphate main chain vibrations of RNA*,phosphate monoesters

ν: stretching vibrations, δ: bending vibrations, s: symmetric, as: asymmetric.

The β-turn protein sub-band at 1638 cm^{-1} was only seen in the control group, while it was absent in all other tested groups. The percentage area of the sub-bands around 1610, 1619, 1645, 1651, 1659, 1667, 1673, 1681and 1695 cm^{-1} increased clearly in the $AlCl_3$ group only compared to the Cont and the other LS treated groups. The β-sheet protein sub-band around 1629.5 cm^{-1}, in the Cont and LS group, was shifted toward the higher frequency in all AD groups which comprise $AlCl_3$, Cure and Prot groups. Another valuable shift in the α-helix sub-band at 1651.9 cm^{-1} was observed for the Cont, Cure, Prot, and LS groups in opposition to the $AlCl_3$ group. This sub-band shifted toward the lower frequency in the $AlCl_3$ group, it was detected at 1649.9 cm^{-1}.

A spectacular shift in the β-sheet protein sub-band was also detected in $AlCl_3$ group toward the higher frequency at 1674.3 cm^{-1} compared to the control at 1673.6 cm^{-1} and the other LS tested groups. By contrast, a marked shift in the β-anti-parallel pleated sheet protein sub-band centred at 1695.8 cm^{-1} for the Cont group toward the lower frequency at 1692.2 cm^{-1} for the $AlCl_3$ group was recorded. This shift was not significant for the other LS treated groups compared to the control.

Internal area ratios were calculated and given in Table 3 to explore biophysical marker for AD against the Cont and to follow up the treatment of LS. All these ratios showed marked differences between the control and the $AlCl_3$ group in one hand and between the LS treated groups and the $AlCl_3$ group in the other hand. The 1641/1695 cm-^{1} and 1659/1695 cm^{-1} ratios represent the formation of random coil and α -helix protein structure to the formation of antiparallel beta structure respectively. Together with alpha/ β sheet ratio, all these ratios showed a dramatic decrease in their values compared to the control in the $AlCl_3$ group. By contrast, these ratios increased drastically to approach nearly the control values in all LS treated groups. The A1641/1651 cm^{-1} ratio increased in the $AlCl_3$ group although both area % of alpha helix and random coil were also increased. For Cure and Prot groups, this ratio markedly decreased while it increased drastically in the LS group. By contrast, the A1673 cm^{-1}/A1695 cm^{-1} ratio showed severe reduction in its value upon $AlCl_3$ intoxication. This ratio increased gradually in the Cure and then in the Prot groups which are AD groups receiving LS for four and eight weeks respectively. While, for LS only group the value of this ratio is comparable to the Cont value.

To distinguish statistically between the Cont, $AlCl_3$, Cure, Prot, and the LS groups and to support the above mentioned results, cluster analysis was carried (Fig. 2). The dendrogram showed a clear segregation between the Cont and the Cure groups on one side and between the Prot, $AlCl_3$, and LS treated groups on the other side. In the cluster, average spectra of Prot, $AlCl_3$, and LS hippocampus tissue two sub-clusters were distinguished; cluster (LS and $AlCl_3$) and cluster Prot group.

3.2. Histological studies

Congo red stain was used, and it stains the nucleoli of the hippocampal neurons only (Fig. 3 Cont). In $AlCl_3$ induced AD rat hippocampus, a significant marked degenerative change was observed in the hippocampal neurons. Most cells appeared smaller, shrunk and deformed. They had a dark cytoplasm and small dark (pyknotic) nuclei which also stained deeply by Congo red. The most affected region was CA3 (Fig. 3a.$AlCl_3$). Individual variation was observed regarding the amount and extent of neuron degeneration. Congo red showed positive staining (Fig. 3b, c.$AlCl_3$).

In the curative group, rats were given $AlCl_3$ for eight weeks and LS water extract was administrated after the fourth week up to the end of the experiment for the last 4 weeks. Treating rats with LS produced potential protection against $AlCl_3$ induced neuronal degeneration in rat hippocampus. The amount of degenerated cells showed a marked decrease compared to non-treated group. In addition, the intensity of Congo red stained cells was decreased. Individual variation observed regarding the degree of response to treatment was guided by the frequency of degenerated cells (Fig. 3a-c Cure).

Administration of $AlCl_3$ together with LS water extract for 8 weeks in the Prot group resulted in marked amioleration of degenerative changes induced by $AlCl_3$. Hippocampal neurons looked more or less similar to those of the control. Degenerated neurons were found to be more frequent compared to the Cure group (Fig. 3. Prot).

Administration of LS water extract to rats did not alter the normal structure of the hippocampal neurons. The cell layers became thicker and the cells looked normal with vesicular nuclei and light stained nuclei (Fig. 3 LS).

4. Discussion

The protein mis-folding and its aggregation may disrupt the cellular membrane and cell function leading to cell death and many diseases including AD, Parkinson's disease, and diabetes type II (Ramirez-Alvarado, Kelly, & Dobson, 2010). The mis-folding of Aβ proteins in AD leads to amyloid plaques, and the structural changes associated with hyper phosphorylation of the tau protein leads to the formation of NFTs (tau proteins) in the gray matter areas of the brain (Miller, Bourassa, & Smith, 2013). This is a result of transformation of small peptide (amyloid-beta) from the soluble α-helix to the insoluble β-fibrillary form (Ii, 1995; Zhang and Rich, 1997).

The neurotoxicity of Aβ peptides is induced by small changes in the A β42 to A β40 ratio and is more vital for the induction of neurotoxicity rather than the absolute amount of Aβ peptides (Hardy & Selkoe, 2002; Kuperstein, Broersen, & Benilova, 2010).

The above reported findings agree with the calculated drastic decrease in the insoluble to soluble IR protein ratio (A1673 cm^{-1}/A1695 cm^{-1}) obtained from our study upon $AlCl_3$ intoxication. This ratio may be used as an excellent indicator for the neurotoxicity.

In an oxidized and un-oxidized membrane model, the accumulated protein more completely adopted a β-sheet conformation on oxidized membranes. The sub-bands around 1623 cm^{-1} and a smaller feature at 1685 cm^{-1} are a spectral signature of anti-parallel β-sheet conformation, most likely represents intermolecular or intramolecular formation of anti-parallel β-sheet by Aβ42 and it is oriented parallel to the membrane plane (Koppaka & Axelsen, 2000).

The relatively narrow HBW of the (amide I band) at 1657 cm^{-1} is

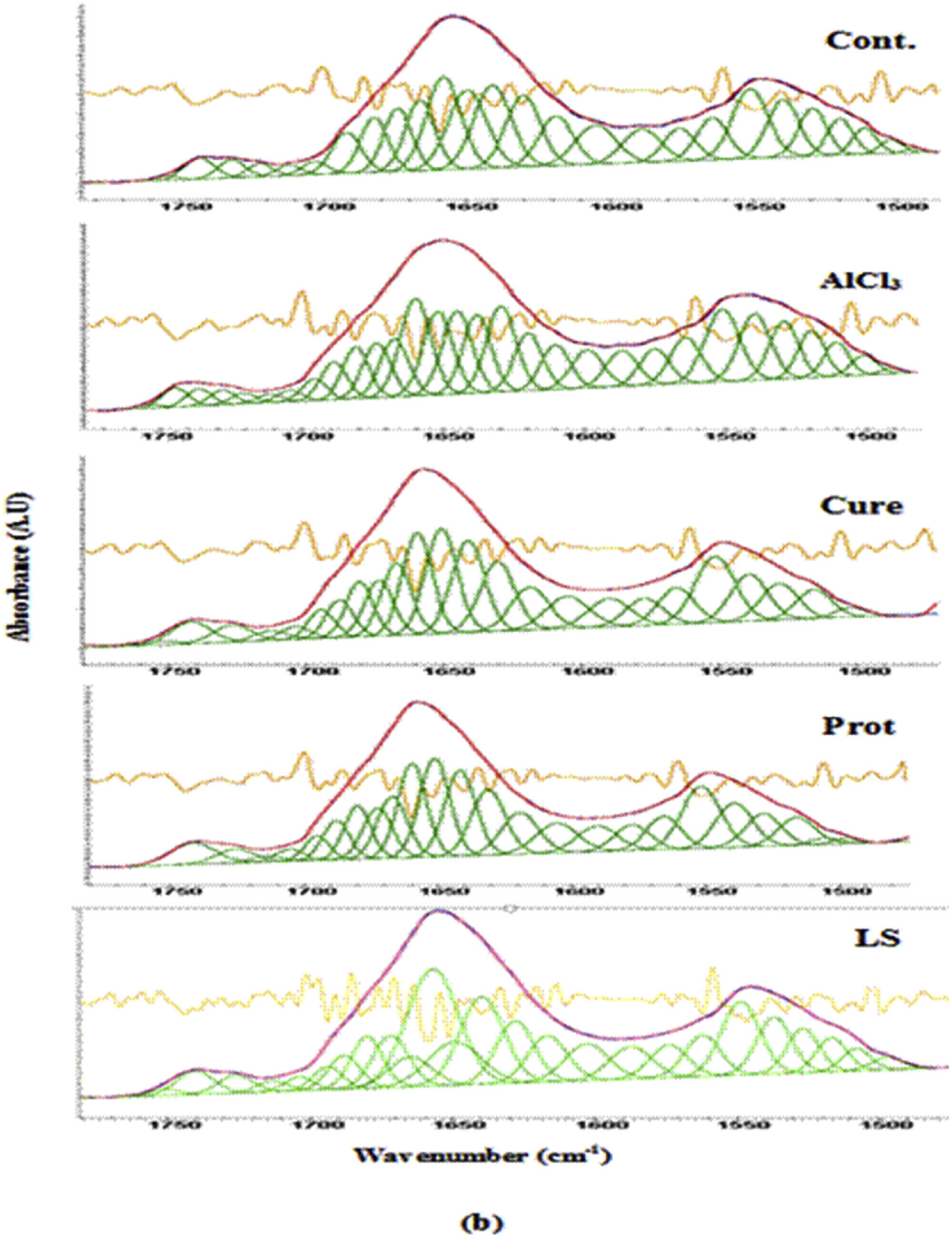

Fig. 1. The ATR-IR Curve fitting of rat hippocampus brain tissues of Cont, $AlCl_3$, Cure, Prot, and LS groups over ester, amide I and amide II 1600-1800 cm^{-1} spectral range.

indicative of a stable and/or long β-strands and strong hydrogen bonds (Goormaghtigh, Cabiaux, & Ruysschaert, 1994). Cerf et al. (2009) examined the secondary structure of both oligomeric and fibrillary Aβ-(1–42) species using ATR-FTIR spectroscopy and demonstrated that these entities adopt a different structure.

In our study, according to the above mentioned discussion, it is evident that the formation of both extracellular soluble parallel and intracellular anti-parallel insoluble Aβ proteins of AD were detected by the increase in the sub-bands area around 1695 and 1673 cm^{-1} respectively for the $AlCl_3$ group compared to the control. Other types of

Table 2
The ATR-IR percentages area of amide I sub- bands together with their assignment of the hippocampus rat brain tissue for all tested groups.

Wave number/Groups	Cont	$AlCl_3$	Cure	Prot	LS	Assignment
1604-1611	1610.13	1605.07	1605.08	1605.67	1604.79	Aromatic Ring
	5.905 ± .0755	7.231 ± .2032[b]	6.317 ± .0755	6.261 ± .1622	6.468 ± .1267 [b]	
1618-1620	1619.79	1618.86	1618.67	1619.49	1618.381	β-turns
	7.455 ± .0892	7.8197 ± .0972	7.403 ± .1037	7.774 ± .0432[b]	7.370 ± .0700 [b]	
1629-1632	1629.48	1630.37	1630.48	1631.34	1629.65	β-sheet
	11.843 ± .1337	11.436 ± .0805	11.078 ± .0767[b]	11.266 ± .19 [b]	9.665 ± .0832 [b]	
1638	1638.07					Random
	10.245 ± .0485					
1641-1646	1645.08	1641.11	1641.13	1641.84	1641.18	Random
	11.515 ± .0829	14.263 ± .0330[b]	13.877 ± .0796[b]	13.571 ± .086[b]	15.776 ± .0632 [b]	
1649-1652	1651.90	1649.88	1650.90	1651.38	1650.66	alph –helix
	11.448 ± .1835	14.028 ± .1273[b]	15.248 ± .0628[b]	15.008 ± .017[b]	9.391 ± .0271 [b]	
1658-1660	1659.85	1658.19	1659.63	1659.88	1658.27	alph helix
	13.725 ± .1059	14.890 ± .0735[b]	13.993 ± .0362[b]	13.664 ± .012	24.790 ± .0156 [b]	
1666-1668	1667.36	1666.42	1667.23	1667.24	1666.10	β-Turns
	7.613 ± .05659	9.574 ± .0612 [b]	9.857 ± .1669 [b]	9.323 ± .0273[b]	5.154 ± .07048 [b]	
1672-1675	1673.61	1674.26	1673.54	1672.71	1672.86	Parallel β-sheet
	7.050 ± .0469	8.150 ± .04946[b]	7.315 ± .0099 [b]	7.506 ± .0233[b]	7.584 ± .4175 [b]	
1680-1683	1681.04	1682.48	1680.65	1680.29	1681.14	antiparullr
	6.212 ± .057	7.010 ± .0140 [b]	6.788 ± .0607 [b]	7.199 ± .0244	6.693 ± .0752 [b]	β-sheet
1687-1690	1688.88		1687.88	1688.23	1689.08	β-sheets
	4.520 ± .0468		4.683 ± .0188	5.371 ± .0371[b]	4.416 ± .0166	
1692-1695	1695.82	1692.23	1694.52	1695	1694.79	Anti-parallel β-sheets
	2.693 ± .0521[b]	3.058 ± .0412[b]	3.442 ± .0353[b]	5.597 ± .0087[b]	2.469 ± .0270	

Values are means ± SEM for three rats each per group. Significance at $P < 0.05$. **b** = significant with the control group.

proteins secondary structure, such as α-helix and random coil, are also present in the rat hippocampus tissue.

The observed increase in the HBW of the β-protein sub-bands around 1641, 1651, 1659 cm^{-1} and the detected decrease in this value for the 1673 cm^{-1} sub-band in AD group may be attributed first to the fact that the misfolding of proteins and the Aβ formation is a slow process that passes through intermediate form (Axelsen, Komatsu, & Murray, 2011; Hilpert, Guba, & Woltering, 2013). The increase in the HBW means the breaking of the hydrogen bonds that stabilize the protein conformational structure and /or the reduction of the β-strand length and hence the denaturation of proteins (Cerf, Sarroukh, & Tamamizu-Kato, 2009). On the other hand, the marked increase in the random coil area percentage suggested that Aβ formation predominantly occurs through random coil transit formation in the $AlCl_3$ group (Axelsen et al., 2011; Hilpert et al., 2013). Second, the detected narrowing and the decrease in the HBW of the insoluble Aβ 1673 cm^{-1} band, by contrast, may indicate that the intracellular proteins are very stable due to hydrogen bonding 25. For all LS treated groups, the drastically increased in the 1651 cm^{-1} sub-band % area over 1659 cm^{-1} and the marked decreased in the formation of Aβ proteins, indicated by the observed decrease in their % area, may suggest that after LS administration the protein re-naturation occurred through α-helix transit phase, the major transit alpha-helix form was centred at 1651 cm^{-1}.

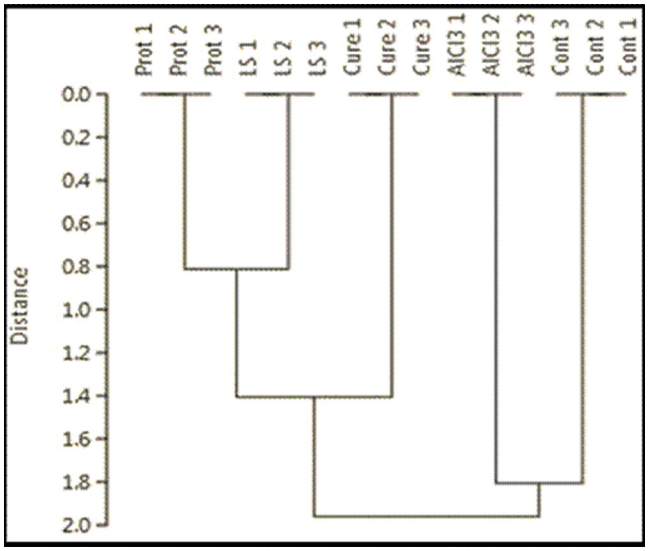

Fig. 2. HCA spectral analysis of the amide regions of the hippocampus brain tissue taken from Cont., $AlCl_3$, Cure, Prot., and LS groups. Ward's, method, Euclidean distances.

Table 3
IR area ratios; quantitative measurements of the Amide I region and its sub-bands specific % area ratios.

Area Ratios/Groups	Cont.	$AlCl_3$	Cure	Prot	LS
A 1673 cm^{-1}/A1695 cm^{-1}	2.8554 ± .172a	1.4562 ± .043 [b]	2.1249 ± .069	2.4548 ± .057	2.8160 ± .048
A1641 cm^{-1}/1695 cm^{-1}	4.6638 ± .614	2.548 ± .246 [b]	4.0317 ± .047	4.4379 ± .614	5.8582 ± .007[b]
A1641 cm^{-1}/ A 1651 cm^{-1}	1.0058 ± .098	1.0167 ± .048	.9101 ± .007	.9042 ± .071	1.6799 ± .0500 [b]
A 1659 cm^{-1}/A 1695 cm^{-1}	5.5582 ± 1.074	2.6603 ± .071[b]	4.0650 ± .146	4.4683 ± .314	9.2081 ± .532[b]
Alpha(1651 cm^{-1} + 1659 cm^{-1}) /beta(1695 cm^{-1} + 1673 cm^{-1} + 1681 cm^{-1})	1.6001 ± .125	1.3931 ± .020[b]	1.6661 ± .122	1.6143 ± .055	2.0141 ± .195b

Values are means ± SEM for three rats per each group. Significance at $p < 0.05$. b = significant with the control group.

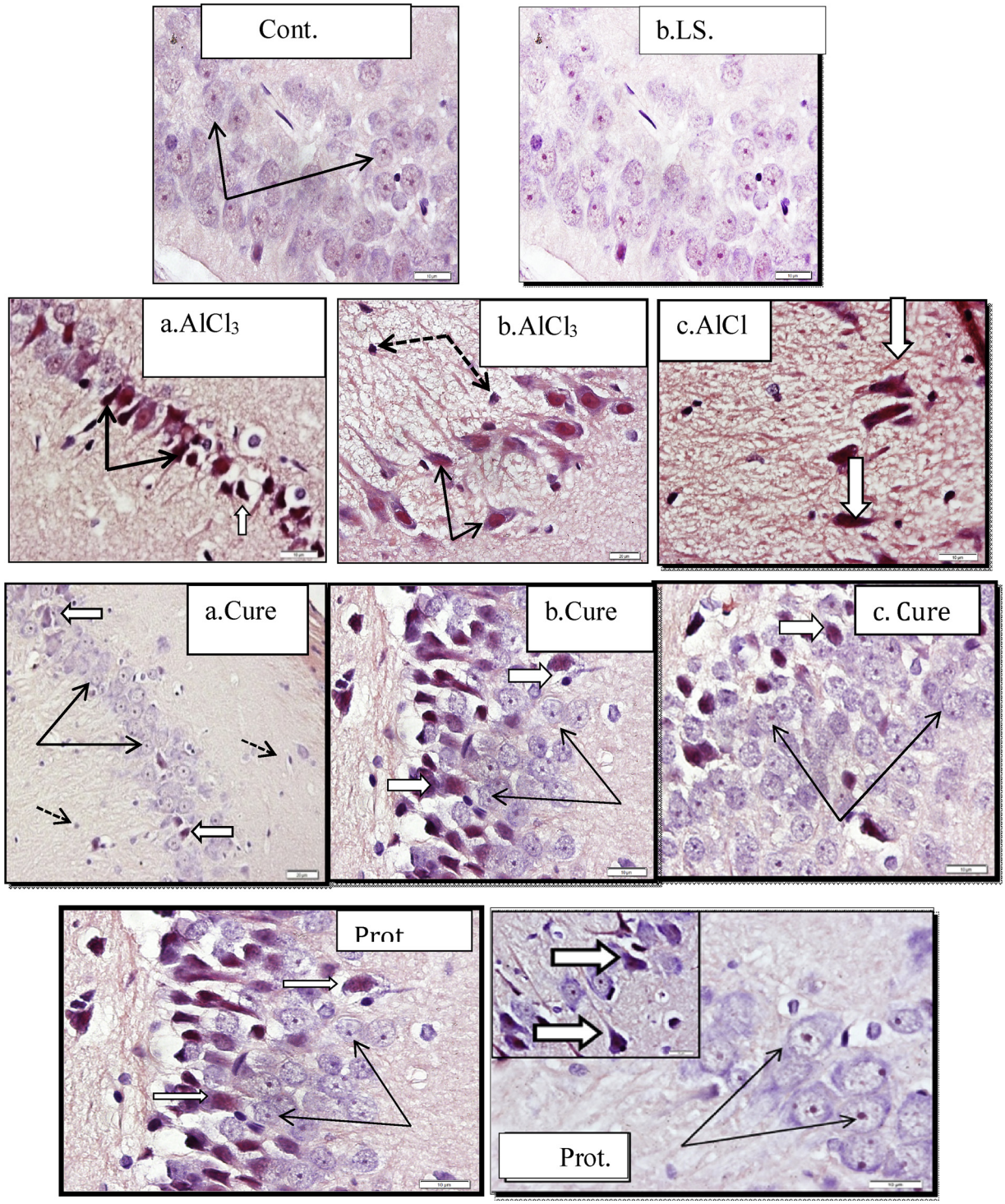

Fig. 3. Sections from rat hippocampus showing: control: with normal large neurons with vesicular large nuclei and light stained cytoplasm (arrows)10 μm. (LS) group showing with few degenerated cells. (a. $AlCl_3$) group showing most neurons shrunken and dark cytoplasm and nuclei (black arrows). Some are surrounded by empty space (white arrow)10 μm. (b. $AlCl_3$) Congo-red stained sections showed dark stained cytoplasm and nuclei (arrows). (c. $AlCl_3$) group with marked loss of neurons (stars). The remaining are shrunken, degenerated, and stained dark by Congo red (white arrows).20 μm. (a–c Cure) showing variation in the degree of preservation of normal neurons (black arrows). However, in most cases, few cells were degenerated (white arrows)10 μm. (Prot.) group starting from the first day of experiment showing preservation of neuronal structure (black arrows) with few degenerated cells in some regions (white arrows) (Congo red stain) 10 μm (For interpretation of the references to colour in this figure legend, the reader is referred to the web version of this article).

The significant decrease in this band % area in the LS group may indicate that there is no need for transit alpha helix for Aβ formation in the LS group. The well-stabilized alpha helix form is now at 1659 cm^{-1} which had the highest % area among the tested groups and even the control. The broadening of these sub-bands was also observed in the Cure and Prot groups even they had lower magnitudes than that detected in the $AlCl_3$ group. This may refer to the continuous formation and aggregation of Aβ-structure. This may suggest that re-naturation of protein mis-folded is predominantly by a transit alpha helix formation mainly of the extra soluble protein at 1695 cm^{-1}. Another different

pathway of the renaturation of protein through transit random coil was present as well. Interestingly, the more resistant, dense core insoluble Aβ protein which is presented by the sub-band around 1673 cm^{-1} showed an increase in its HBW in all LS treated groups. This indicates the breaking in the hydrogen bonding that stabilize its structure and may suggest the re-solubilisation of this Aβ tau protein (Cerf et al., 2009). These findings are also supported by the results obtained from the calculated amide I sub-bands area ratios (A 1641/ A1651 cm^{-1}; A 1641/A1695 cm^{-1}, A1659/A 1695 cm^{-1} and alpha/ β) which can be used as excellent biophysical markers of the degree of Aβ formation through transit phase. The same trend was detected in the calculation of these sub-band percentage area ratios for Raman decomposing amide I band for the same hippocampus tissues (data not shown). The animals that received only LS had no intention for Aβ formation and both Aβ % areas of this group had nearly comparable values as the control.

Histopathological results supported strongly the findings obtained by ATR-IR results. Congo red is a stain known to be specific for detection deposition of amyloid substance in tissues (Liu, Lan, & Zhao, 2014). Changes observed by Congo red were similar to what was reported previously in the available literature describing $AlCl_3$ induced AD (Walton & Wang, 2009).

LS is known for its traditional use as a medicinal plant comprises Sinapic acid and silicon (Si) as metal chelator (Raouf, Gashlan, Khedr, and Al-Jabbri, 2015; Eddouks, Maghrani, Zeggwagh, and Michel, 2005). Sinapic acid showed antioxidant, antimicrobial, anti-inflammatory, anticancer, and anti-anxiety activity. With its derivatives-sinapine (sinapoyl choline), it acts as an acetylcholinesterase inhibitor which might have therapeutic uses in some disease like AD (Nićiforović & Abramovič, 2014).

Si potentially reduces AD risk and greatly supports cognitive function (Gillette Guyonnet, Andrieu, & Vellas, 2007). Si markedly decreases Al absorption from the human digestive track and a decrease in its accumulation in brain when subjects were treated with soluble silicon (Dong, Atwood, & Anderson, 2003; Jurkić, Cepanec, Pavelić, & Pavelić, 2013).

5. Conclusion

We postulated the formation of Aβ extracellular proteins through random coil transit phase, and the re-solubilisation of the NFTs through alpha helix transit phase in response to LS water extract treatment. The mis-folding of proteins, proteins aggregation and the changes in their secondary structure were evident upon Al intoxication by both spectral and histological studies.

Conflict of interest

The authors declare that they have no financial or non-financial competing interests.

Ethical statement

The current study was approved by the Animal House, King Fahd Medical Research Centre, King Abdulaziz University. All applicable international, national and/or institutional guidelines for the care and use of animals were followed.

Funding

This research work was supported by King Abdulaziz City for Science and Technology; grant number: AT-145-34 - KSA.

Acknowledgment

This research work was supported by King Abdulaziz City for Science and Technology; grant number: AT-145-34- Riyadh- KSA.

Appendix A. Supplementary data

Supplementary material related to this article can be found, in the online version, at doi:https://doi.org/10.1016/j.npbr.2018.11.001.

References

Abeysekara, S., Damiran, D., & Yu, P. (2013). Univariate and multivariate molecular spectral analyses of lipid related molecular structural components in relation to nutrient profile in feed and food mixtures. *Spectrochimica Acta - Part A: Molecular and Biomolecular Spectroscopy, 102*, 432–442. https://doi.org/10.1016/j.saa.2012.09.064.

Akkas, S. B., Inci, S., Zorlu, F., & Severcan, F. (2007). Melatonin affects the order, dynamics and hydration of brain membrane lipids. *Journal of Molecular Structure, 834-836*, 207–215. https://doi.org/10.1016/j.molstruc.2006.12.018 SPEC. ISS.

Axelsen, P. H., Komatsu, H., & Murray, I. V. J. (2011). Oxidative stress and cell membranes in the pathogenesis of Alzheimer's disease. *Physiology (Bethesda, Md), 26*(1), 54–69. https://doi.org/10.1152/physiol.00024.2010.

Balgoon, M. J., Raouf, G. A., Qusti, S. Y., & Ali, S. S. (2015). ATR-IR study of the mechanism of aluminum chloride induced Alzheimer's disease ; curative and protective effect of lipidium sativum water extract on hippocampus rats brain tissue. *International Journal of Medical, Health, Biomedical, Bioengineering and Pharmaceutical Engineering, 9*(11), 782–792.

Cakmak, G., Zorlu, F., Severcan, M., & Severcan, F. (2011). Screening of protective effect of amifostine on radiation-induced structural and functional variations in rat liver microsomal membranes by FT-IR spectroscopy. *Analytical Chemistry, 83*(7), 2438–2444. https://doi.org/10.1021/ac102043p.

Cerf, E., Sarroukh, R., Tamamizu-Kato, S., et al. (2009). Antiparallel β-sheet: A signature structure of the oligomeric amyloid β-peptide. *The Biochemical Journal, 421*(3), 415–423. https://doi.org/10.1042/BJ20090379.

Dong, J., Atwood, C. S., Anderson, V. E., et al. (2003). Metal binding and oxidation of amyloid-β within isolated senile plaque cores: Raman microscopic evidence. *Biochemistry, 42*(10), 2768–2773. https://doi.org/10.1021/bi0272151.

Downie, T. (1990). Theory and practice of histological techniques Edited by J.D. Bancroft & A. Stevens, Churchill Livingstone, Edinburgh, 740 pages,? ?55.00. *Histopathology, 17*(4), https://doi.org/10.1111/j.1365-2559.1990.tb00755.x 386-386.

Drury, R., & Wallington, E. (1980). *Carleton's histological technique* (5th ed.). Oxford: Oxford University Press188–291.

Eddouks, M., Maghrani, M., Zeggwagh, N. A., & Michel, J. B. (2005). Study of the hypoglycaemic activity of Lepidium sativum L. aqueous extract in normal and diabetic rats. *Journal of Ethnopharmacology, 97*(2), 391–395. https://doi.org/10.1016/j.jep.2004.11.030.

Esparza, J. L., Gomez, M., Rosa Nogues, M., Paternain, J. L., Mallol, J., & Domingo, J. L. (2005). Melatonin reduces oxidative stress and increases gene expression in the cerebral cortex and cerebellum of aluminum-exposed rats. *Journal of Pineal Research, 39*(2), 129–136 JPI225[pii]\r10.1111/j.1600-079X.2005.00225.x.

Forina, M., Armanino, C., & Raggio, V. (2002). Clustering with dendrograms on interpretation variables. *Analytica Chimica Acta, 454*(1), 13–19. https://doi.org/10.1016/S0003-2670(01)01517-3.

Gillette Guyonnet, S., Andrieu, S., & Vellas, B. (2007). The potential influence of silica present in drinking water on Alzheimer's disease and associated disorders. *The Journal of Nutrition, Health & Aging, 11*(2), 119–124. http://ovidsp.ovid.com/ovidweb.cgi?T=JS&PAGE=reference&D=med5&NEWS=N&AN=17435954.

Goormaghtigh, E., Cabiaux, V., & Ruysschaert, J.-M. (1994). *Determination of soluble and membrane protein structure by Fourier transform infrared spectroscopy. Physicochemical methods in the study of biomembranes*405–450. https://doi.org/10.1007/978-1-4615-1863-1_10.

Haass, C., Kaether, C., Thinakaran, G., & Sisodia, S. (2012). Trafficking and proteolytic processing of APP. *Cold Spring Harbor Perspectives in Medicine, 2*(5), https://doi.org/10.1101/cshperspect.a006270.

Hardy, J., & Selkoe, D. J. (2002). The amyloid hypothesis of Alzheimer's disease : progress and problems on the road to therapeutics. *Science, 297*(July), 353–357. https://doi.org/10.1126/science.1072994.

Hilpert, H., Guba, W., Woltering, T. J., et al. (2013). β-Secretase (BACE1) inhibitors with high in vivo efficacy suitable for clinical evaluation in Alzheimer's disease. *Journal of Medical Chemistry, 56*, 3980–3995. https://doi.org/10.1021/jm400225m.

Ii, K. (1995). The role of β-amyloid in the development of Alzheimer's disease. *Drugs & Aging, 7*(2), 97–109. https://doi.org/10.2165/00002512-199507020-00004.

Jurkić, L. M., Cepanec, I., Pavelić, S. K., & Pavelić, K. (2013). Biological and therapeutic effects of ortho-silicic acid and some ortho-silicic acid-releasing compounds: New perspectives for therapy. *Nutrition and Metabolism, 10*(1), https://doi.org/10.1186/1743-7075-10-2.

Koppaka, V., & Axelsen, P. H. (2000). Accelerated accumulation of amyloid? ? proteins on oxidatively damaged lipid membranes. *Biochemistry, 39*(32), 10011–10016. https://doi.org/10.1021/bi000619d.

Korte, M., Herrmann, U., Zhang, X., & Draguhn, A. (2012). The role of APP and APLP for synaptic transmission, plasticity, and network function: Lessons from genetic mouse models. *Experimental Brain Research, 217*(3-4), 435–440. https://doi.org/10.1007/s00221-011-2894-6.

Kumar, V., & Gill, K. D. (2014). Oxidative stress and mitochondrial dysfunction in aluminium neurotoxicity and its amelioration: A review. *NeuroToxicology, 41*, 154–166. https://doi.org/10.1016/j.neuro.2014.02.004.

Kumar, V., Bal, A., & Gill, K. D. (2008). Impairment of mitochondrial energy metabolism in different regions of rat brain following chronic exposure to aluminium. *Brain*

Research, 1232, 94–103 S0006-8993(08)01715-0[pii]\r10.1016/j.brainres.2008.07.028.

Kumar, V., Bal, A., & Gill, K. D. (2009). Aluminium-induced oxidative DNA damage recognition and cell-cycle disruption in different regions of rat brain. *Toxicology, 264*(3), 137–144. https://doi.org/10.1016/j.tox.2009.05.011.

Kuperstein, I., Broersen, K., Benilova, I., et al. (2010). Neurotoxicity of Alzheimer's disease Aβ peptides is induced by small changes in the Aβ42 to Aβ40 ratio. *The EMBO Journal, 29*(19), 3408–3420. https://doi.org/10.1038/emboj.2010.211.

Liu, J., Lan, J., Zhao, P., et al. (2014). Evidence of the presence of amyloid substance in the blood of familial amyloidotic polyneuropathy patients with ATTR Val30Met mutation. *International Journal of Clinical and Experimental Pathology, 7*(11), 7795–7800.

Miller, L. M., Bourassa, M. W., & Smith, R. J. (2013). FTIR spectroscopic imaging of protein aggregation in living cells. *Biochimica et Biophysica Acta, 1828*(10), 2339–2346. https://doi.org/10.1016/j.bbamem.2013.01.014.

Nićiforović, N., & Abramovič, H. (2014). Sinapic acid and its derivatives: Natural sources and bioactivity. *Comprehensive Reviews in Food Science and Food Safety, 13*(1), 34–51. https://doi.org/10.1111/1541-4337.12041.

Palaniappan, P. R., & Vijayasundaram, V. (2009). The FT-IR study of the brain tissue of Labeo rohita due to arsenic intoxication. *Microchemical Journal, 91*(1), 118–124. https://doi.org/10.1016/j.microc.2008.08.014.

Ramirez-Alvarado, M., Kelly, J. W., & Dobson, C. M. (2010). Protein Misfolding Diseases. *Current and Emerging Principles and Therapies*. https://doi.org/10.1002/9780470572702.

Raouf, G. A., Gashlan, H., Khedr, A., & Al-Jabbri, H. (2015). In vitro new biopolymer for bone grafting and bone cement. *International Journal of Latest Research in Science and Technology, 4*(2), 46–55.

Sethi, P., Jyoti, A., Singh, R., Hussain, E., & Sharma, D. (2008). Aluminium-induced electrophysiological, biochemical and cognitive modifications in the hippocampus of aging rats. *NeuroToxicology, 29*(6), 1069–1079. https://doi.org/10.1016/j.neuro.2008.08.005.

Shati, A. A., Elsaid, F. G., & Hafez, E. E. (2011). Biochemical and molecular aspects of aluminium chloride-induced neurotoxicity in mice and the protective role of Crocus sativus L. extraction and honey syrup. *Neuroscience, 175*, 66–74. https://doi.org/10.1016/j.neuroscience.2010.11.043.

Walton, J. R., & Wang, M. X. (2009). APP expression, distribution and accumulation are altered by aluminum in a rodent model for Alzheimer's disease. *Journal of Inorganic Biochemistry, 103*(11), 1548–1554. https://doi.org/10.1016/j.jinorgbio.2009.07.027.

Zhang, S., & Rich, A. (1997). Direct conversion of an oligopeptide from a beta-sheet to an alpha-helix: a model for amyloid formation. *Proceedings of the National Academy of Sciences of the United States of America, 94*(January), 23–28. https://doi.org/10.1073/pnas.94.1.23.